Journal of Hazardous Materials 211–212 (2012) 288–295

Contents lists available at SciVerse ScienceDirect

Journal of Hazardous Materials

journal homepage: www.elsevier.com/locate/jhazmat

Functionalized nanoparticle interactions with polymeric membranes

D.A. Ladner[a,*], M. Steele[a], A. Weir[b], K. Hristovski[b,c], P. Westerhoff[b]

[a] Clemson University, Department of Environmental Engineering and Earth Sciences, Clemson, South Carolina, USA
[b] Arizona State University, School of Sustainable Engineering and the Built Environment, Tempe, Arizona, USA
[c] Arizona State University, Polytechnic Campus, College of Technology and Innovation, Mesa, Arizona, USA

ARTICLE INFO

Article history:
Received 16 May 2011
Received in revised form
13 November 2011
Accepted 14 November 2011
Available online 23 November 2011

Keywords:
Microfiltration
Ultrafiltration
Adsorption
Separation
Fouling

ABSTRACT

A series of experiments was performed to measure the retention of a class of functionalized nanoparticles (NPs) on porous (microfiltration and ultrafiltration) membranes. The findings impact engineered water and wastewater treatment using membrane technology, characterization and analytical schemes for NP detection, and the use of NPs in waste treatment scenarios. The NPs studied were composed of silver, titanium dioxide, and gold; had organic coatings to yield either positive or negative surface charge; and were between 2 and 10 nm in diameter. NP solutions were applied to polymeric membranes composed of different materials and pore sizes (ranging from ~2 nm [3 kDa molecular weight cutoff] to 0.2 μm). Greater than 99% rejection was observed of positively charged NPs by negatively charged membranes even though pore diameters were up to 20 times the NP diameter; thus, sorption caused rejection. Negatively charged NPs were less well rejected, but behavior was dependant not only on surface functionality but on NP core material (Ag, TiO_2, or Au). NP rejection depended more upon NP properties than membrane properties; all of the negatively charged polymeric membranes behaved similarly. The NP-membrane interaction behavior fell into four categories, which are defined and described here.

1. Introduction

Engineered nanoparticles (NPs) are finding increased use in consumer products such as clothing, children's toys, household products, and personal care products [1–4]. The Woodrow Wilson International Center for Scholars found 212 nanomaterial-containing products on the market in 2006 and more than 1000 in 2009 [5]. Environmental fate models predict that many NPs will come into contact with and be conveyed by sewage and storm water [6–8]. Laboratory tests have demonstrated NP release from consumer products and during clothes washing [1,2], and NPs have been found in wastewater treatment plant effluents [9,10]. Discharges from NP manufacturing facilities are also likely to be an important point source of environmental NPs [11].

In addition to the potentially negative impacts noted above, NPs also have positive environmental uses when employed to remediate other contaminants. Often the NPs must be retained in the treatment system, such as when they are used as catalysts. TiO_2 and zero-valent iron are two NP materials with remediation capabilities for which retention in the system is desired [12,13].

Membrane processes are a potentially viable technology for removing or retaining engineered NPs [14–17]. Much of the information available on nanoparticle (colloid) interactions with membranes comes from studies in which membrane fouling is of interest [18–22]. In those cases the NPs (colloids) are meant to represent naturally occurring material and are typically larger than the membrane pores. NP removal by microfiltration (MF) and ultrafiltration (UF) membranes in which the NPs are smaller than the pores has been studied for a few NP types and membrane materials. For example, rejection of silver colloids (2–20 nm, mean 8 nm) was tested on 30-, 100-, and 300-kDa polysulfone and 0.22-μm PVDF membranes [23]. Particles were well rejected by the tighter membranes, but even the looser PVDF membrane demonstrated some particle removal. Silver (8.3 nm) and gold (10 nm) colloids were shown to adsorb to porous membranes, which enabled visualization of fouling phenomena [24]. Adsorption was also important in the rejection of colloidal hematite (75, 250, and 500 nm) by 0.22-μm MF membranes [25]. Rejection decreased with several membrane backwash cycles, presumably because adsorption sites were filled in early stages. Adhesion of NPs to membranes can be strong, as demonstrated by silica colloids that bound more readily than polystyrene colloids [22]. NP aggregation is also an important mechanism of rejection, as has been demonstrated with hematite [26] and more recently with magnetic $CoFe_2O_4$ NPs [27].

NP separation using UF membranes has received attention as a means for NP characterization. For example, UF was used for differentiation between ZnO NPs and dissolved Zn^{2+} in toxicity studies [28]. Separation of ionic and NP forms of silver has also been reported [29]. Other groups have similarly purified Au [30] and iron oxide [31,32] during NP synthesis. Another need in the

* Corresponding author. Tel.: +1 864 656 5572; fax: +1 864 656 0672.
E-mail address: ladner@clemson.edu (D.A. Ladner).

0304-3894/$ – see front matter © 2011 Elsevier B.V. All rights reserved.
doi:10.1016/j.jhazmat.2011.11.051

Table 1
NP characteristics. Each is designated by its core inorganic material followed by its surface charge in parentheses. Size is the median particle size determined by PALS.

Designation	Size (nm)	Functionalizing polymer
Ag(−)	6–7	Polyacrylate
TiO_2(−)	4–5	Polyacrylate
Au(−)	6–7	Polyacrylate
Au(+)	6–7	Poly(quaternary ammonium)
TiO_2(+)	5–7	Poly(quaternary ammonium)

environmental research field is to collect and concentrate environmental NPs. A review covering aquatic environmental NPs described several workers using UF and tangential-flow UF to collect NPs [33]. One group developed an automated UF device that concentrates NPs with various membranes [34]. In these reports on NP separation and collection from environmental matrices, membrane pore sizes well below the NP size are typically chosen, and little discussion of NP-membrane interactions is included.

Membrane filtration has also been used to remove viruses, which are in the nanometer size range. One group used several UF membranes between 30 and 300 kDa to remove viruses between 18 and 26 nm in size [35]. The 100-kDa membrane was deemed optimal because it effectively rejected viruses while allowing most proteins to pass.

In general, NPs with diameters larger than the membrane pore sizes can be removed, but NPs smaller than the pores can also be removed because of adsorption to membrane surfaces, electrostatic interactions, or other interactions. To fully understand and predict separation behavior, it is important to understand such interactions; however, studies demonstrating these effects are sparse. We found only one study that used a variety of membranes with varying porosity to examine rejection, and in that case the only NP used was colloidal silver, which has a fairly strong adsorption affinity [23]. A more complete set of experiments is warranted to determine the interactions between NPs with varying material properties and polymeric membranes of varying pore size.

This study evaluates the extent to which MF and UF membranes remove engineered NPs with surface coatings (e.g., carboxy or amino functional groups). Solutions containing NPs were applied to a range of polymeric membranes composed of different materials and with varying pore sizes (ranging from ~2 nm [3 kDa molecular weight cutoff] to 0.2 μm). Potential mechanisms for NP removal by the membranes are investigated. The outcome of this research provides valuable information on the use of membranes to remove NPs from waste streams, to prevent their release into the environment, and to size-separate and characterize NPs in environmental samples.

2. Materials and methods

2.1. Nanoparticles

Five NPs of similar hydrodynamic size but different composition and functionality were used: negatively charged silver [Ag(−)], negatively and positively charged titanium dioxide [TiO_2(−) and TiO_2(+)] and gold [Au(−) and Au(+)] NPs (all from Vive Nano, Toronto, ON, Canada). Negatively charged NPs were manufactured with polyacrylate such that the polymer was incorporated into the NP and carboxyl groups imparted a negative surface charge at neutral pH. Positively charged NPs were formed similarly, but with poly(quaternary ammonium). All NPs were between 2 and 9 nm in size as measured by transmission electron microscopy (TEM) and phase analysis light scattering (PALS). PALS data are in Table 1, and TEM images are in Fig. S1. NPs were received in aqueous suspensions and diluted (usually 1000-fold) with 1 mM $NaHCO_3$ to create gently buffered, slightly alkaline working solutions (pH 8.9 ± 0.7) to minimize NP dissolution. The concentration of the working solution (the membrane "feed" sample) was measured in all cases.

2.2. Nanoparticle concentration determination

Nanoparticle concentrations were measured using inductively coupled plasma-optical emission spectroscopy (ICP-OES) on a Thermo iCAP 6300 ICP-OES instrument. Silver and TiO_2 NP samples were acidified prior to testing using 3% by volume HNO_3. Gold samples were acidified with 3% HCl and 1% HNO_3.

The concentration of ionic silver in the stock Ag(−) solution was determined using an ion-selective electrode (Symphony Silver-Sulfide Ion Selective Combination Electrode, VWR). The stock solution was diluted tenfold in 0.1-M $NaNO_3$ to adjust the ionic strength as required for electrode measurements. Silver nitrate solutions between 1 and 100 ppm were used as standards. Measurements of ionic Ag and Ti were not made because of the low solubility of these metals.

2.3. Membranes

A variety of membranes were chosen for this work that represent materials typically used in water and wastewater treatment applications and laboratory sample handling. Membrane details are given in Table 2. The 0.1-μm hydrophilic PVDF membranes are similar in pore size and material to the hollow-fiber membranes most commonly used in full-scale applications. The PVDF material is not itself hydrophilic but was modified by the manufacturer to increase its hydrophilicity. The exact modification procedure used is proprietary, but is likely graft polymerization of a polymerizable monomer such as hydroxyalkyl acrylate or methacrylate [36,37]. The other membranes have pore sizes larger and smaller than the PVDF membrane, and all have negative charge, as is typical in water filtration. Membranes with 0.2-μm pore size are often used to differentiate particulate from dissolved fractions and are considered sufficient for sterile filtration because they remove bacteria. UF membranes are typically used for size separation among proteins as well as for removing polysaccharides and other high-molecular-weight organic matter.

Membrane zeta potential was determined with a SurPASS (Anton Paar GmbH, Graz, Austria) electrokinetic analyzer. Zeta potential was calculated using the Fairbrother-Mastin equation from measured streaming current values. Streaming current was measured as the solution passed through a channel that was 2 cm in length, 1 cm in width, and approximately 100 μm in height; the membrane material served as the top and bottom of the channel. Flow was induced in the measurement cell by linearly ramping the differential pressure from 0 to 400 mbar in both directions. Two cycles of pressure ramping in each direction were conducted, and the average zeta potential was reported. The electrolyte was 0.001 M KCl. HCl (0.1 M) and NaOH (0.1 M) were used to adjust the pH. Before measurements, membranes were placed overnight in deionized water to wet the materials fully and remove processing chemicals. Samples were also rinsed at each pH point before the zeta potential was measured. Zeta potentials are reported in Table 2. For UF membranes, the membrane surface area available in the centrifugal filtration apparatuses was too small for zeta potential measurements, so most of those are not reported. However, separate membrane sheets were obtained from the manufacturer for the 30- and 100-kDa membranes and zeta potentials for those were measured and reported. The other UF membranes are expected to have similar zeta potentials because the material (regenerated cellulose) is the same.

Table 2
Membrane characteristics. Pore sizes for UF membranes (between 3 and 100 kDa MWCO) were estimated using reference [40] assuming the geometric standard deviation of the pore sizes (σ) is 1.4.

Membrane designation	Pore size (MWCO*)	Material	Manufacturer	Model number or filter code	Zeta potential at pH 8.7 (mV)
0.22-μm PS	0.22 μm	Polysulfone	Pall	Gelman 66199	−14
0.22-μm PES	0.22 μm	Polyethersulfone	Pall	Gelman 60301	−22
0.22-μm CA	0.22 μm	Cellulose acetate	GE Osmonics	A02SP	−31
0.22-μm PVDF	0.22 μm	Polyvinylidene fluoride	Millipore	GVWP	−23
0.22-μm Nylon	0.22 μm	Nylon (polyamide)	Not specified (distributor Sigma–Aldrich)	Z290807	−8
0.1-μm PVDF	0.10 μm	Hydrophilic polyvinylidene fluoride	Millipore	VVLP	−17
100-kDa RC	9 nm (100 kDa)	Regenerated cellulose	Millipore	PLHK	−14
50-kDa RC	7 nm (50 kDa)	Regenerated cellulose	Millipore	PLQK	NA
30-kDa RC	5 nm (30 kDa)	Regenerated cellulose	Millipore	PLTK	−34
10-kDa RC	3 nm (10 kDa)	Regenerated cellulose	Millipore	PLGC	NA
3-kDa RC	2 nm (3 kDa)	Regenerated cellulose	Millipore	PLBC	NA

* MWCO, molecular weight cutoff; NA, not available.

2.4. Membrane–NP interaction experiments

2.4.1. Dead-end filtration and rejection over time

The dead-end filtration apparatus (Amicon 8050, Millipore) used 39-mm diameter circular membrane coupons in unstirred mode. Pressure was held constant using a nitrogen cylinder and a regulator connected to a pressure vessel (feed tank). A detailed diagram of the membrane apparatus can be found elsewhere [38] and in Fig. S2. To provide extra support and resistance against membrane deformation, a mesh screen was placed under the coupon. The screen was cut from the permeate carrier of a spiral-wound nanofiltration module (ESNA-1 LF, Hydranautics, Oceanside, CA). Membrane flux was determined by recording the mass of permeate collected over time on a top-loading balance (Model PB3002-S, Mettler-Toledo) using data acquisition software (Labview, National Instruments). Before each NP sample filtration the membrane integrity was verified by measuring the flux of ultrapure (18.2 MΩ-cm) water, which should be within 10% of the average flux recorded for other membranes of that type. Both clean water and NP samples were measured to be at ambient temperature (21 ± 1 °C).

One set of dead-end experiments used a one-liter feed volume at 70 kPa (10 psi), and filtration ran until the feed was below the intake tube (approximately 930 ml total volume filtered). Permeate samples were collected at 5, 10, 15, 20, 400, and 800 ml. Another set of experiments used no feed tank; the sample volume was reduced to 60 ml and placed directly in the membrane cell. The pressure was reduced to 35 kPa (5 psi) to reduce flux and facilitate sample collection; permeate samples were collected in 6-ml increments.

For all membrane experiments, rejection (*Rej*) was calculated as

$$Rej = 1 - \frac{C_p}{C_f} \quad (1)$$

where C_p is the permeate concentration and C_f is the feed concentration. For centrifugal filtration, the recovery (*Rec*) was calculated using

$$Rec = \frac{M_c}{M_f - M_p} = \frac{C_c V_c}{C_f V_f - C_p V_p} \quad (2)$$

where M is the mass of the metal fraction of the NPs in the samples. M was determined using the NP concentration (C) measured by ICP-OES and the measured volume (V). The subscripts c, f, and p denote concentrate, feed, and permeate, respectively. Thus, the recovery as defined here is a ratio of the mass measured in the resuspended concentrate compared to the mass expected in the concentrate; it is a measure of the NPs that did not remain attached to the membrane. High recovery (close to 1) would be expected when NPs and membranes had weak adsorptive interaction potential or were not easily entrapped in the membrane matrix. Low recovery is expected for particles that adsorb strongly to the membrane.

2.4.2. Centrifugal filtration

Centrifugal membrane filters (Amicon Ultra, Millipore; Fig. S3) were used to test NP interactions with regenerated cellulose UF membranes having molecular-weight cutoff (MWCO) values of 3, 10, 30, 50, and 100 kDa. Aliquots of 10 ml of NP solution were added to the filter device (which was held in a 50-ml centrifuge tube) and loaded into a fixed-rotor centrifuge with the membrane face perpendicular to the axis of the rotor. After spinning at 5000 rcf for 15 min, the permeate was weighed and collected for ICP-OES analysis. The concentrate was resuspended with approximately 11 ml of ultrapure water and gently swirled by hand to recover any loosely attached particles from the membrane. This resuspended concentrate was also weighed and collected for ICP-OES.

2.4.3. Syringe filtration

Early experimental results indicated that interactions between negatively charged NPs and 0.22-μm membranes could not be assessed easily when NP solutions were passed once through the membranes; the feed and permeate concentrations were too similar. To achieve greater separations and enable comparisons among NPs and membrane materials, NP samples were passed through the membranes ten times. Syringe filter apparatuses were used to facilitate these experiments. Circular 25-mm diameter membranes were used with an Easy-Pressure Syringe Filter Holder (Pall). Both the feed and permeate sides of the holder were attached to syringes (using a 2-cm Viton tube on the permeate side) such that the sample passed from one syringe to another through the membrane holder. The holder direction was switched for the subsequent passage back to the original syringe so that the direction of filtration through the membrane was the same for all ten steps. Some adsorption to the syringe and/or holder was observed. Thus for the data reported here a pre-adsorption step was used to exhaust the adsorptive capacity of the plastic materials; six aliquots of NP working solution of 6 ml each were passed through the holder five times. Then a membrane was placed in the holder, and a new 6-ml sample of the NP working solution was filtered ten times as described above. The sample was

measured by ICP-OES to determine the NP concentration remaining.

2.4.4. Membrane adsorption

The potential for NPs to absorb to the membranes was tested in static adsorption experiments. NP solution was added to 10-ml vials into which were placed varying amounts of membrane material (from 0 to 8000 mm^2) that was cut into approximately 1-cm^2 pieces. The vials were shaken overnight, and NP concentrations remaining in solution were measured with ICP-OES.

2.5. Imaging of membranes and nanoparticles

NP size was confirmed visually using transmission electron microscopy (TEM) with a Philips CM200 STEM. Samples were placed on 300 mesh formvar-coated copper grids. NP layers on membranes were characterized visually using the scanning electron microscopy/electron dispersive X-ray microanalysis (SEM/EDX) technique (FEI NOVA 200 equipped with the EDAX system). Membrane samples were attached with carbon tape to the SEM stub, and analysis was conducted in backscatter immersion mode to differentiate the heavier nanoparticle elements (e.g. Ag), which appear lighter, from the lighter membrane elements such as carbon, which appear darker.

3. Results and discussion

3.1. Dead-end filtration and rejection over time

Four dead-end filtrations using 0.1-μm PVDF membranes performed with one-liter solutions of Ag(−) NPs had an average Ag rejection of only 4.2% after passage of 800 ml through the membrane. Data collected over time, however, showed that at the very beginning of two experiments (i.e., in the first 5 ml of collection), the membrane retained 36% and 20% of the Ag (Fig. S4). The captured Ag(−) was observed visually by a graying of the white membranes. This was also confirmed by SEM (Fig. S5) and by EDX that gave a strong Ag signal.

Similar 1-L experiments were performed with the other NPs, but adsorption of the particles with positive charge was observed on the metal feed tank and plastic tubing in control experiments with no membrane present. This caused the data (shown in Figs. S6 and S7) to be of limited usefulness. The experimental design was modified such that only 60 ml of solution was used; this quantity fit directly in the membrane cell and thus had minimal exposure to the apparatus surface area.

Results of the 60-ml and 1-L dead-end experiments with Ag(−) at both dilute and higher concentrations were comparable. Fig. 1 shows the results from the 60-mL experiments. For Ag(−), as with 1 L experiments, the 0.1-μm PVDF membranes retained some silver during the first 5–10 mL of applied volume but then the permeate approached feed concentrations (i.e., $[NP]_{permeate}/[NP]_{feed}$ approached 100%). Further analysis using an Ag ion-selective electrode showed that 14% of the detectable Ag in the Ag(−) stock solution was ionic, so the actual NP passage was lower; e.g., where 76% passage was reported at 5 ml in Fig. 1, the NP passage was actually 72%. The membrane retained TiO_2(−) to a slightly greater extent than Ag(−), and it retained significantly more Au(−) than the other negatively charged particles. The positively charged NPs, Au(+) and TiO_2(+), were almost completely retained.

3.2. Adsorption

The above dead-end experiments indicated that NPs with a diameter significantly smaller than the membrane pore size could be prevented from passing through the membrane. As a potential

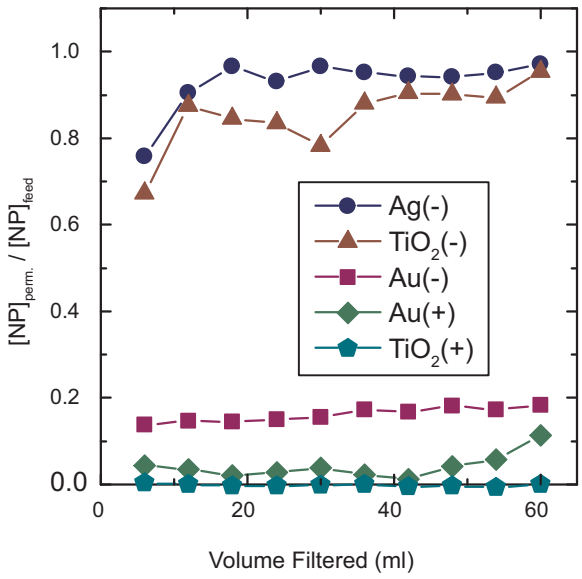

Fig. 1. Normalized rejection versus volume filtered for five NPs on 0.1-μm PVDF membranes with 39-mm active filter diameter. Feed concentrations were 0.76, 0.24, 0.23, 0.12, and 0.13 ppm for Ag(−), TiO_2(−), Au(−), Au(+), and TiO_2(+), respectively.

removal mechanism, sorption of NPs to the membranes was quantified. Fig. 2 illustrates results from batch sorption experiments in which solutions containing NPs were allowed to equilibrate with different sizes of membrane coupons (i.e., variable size) without any flux across or through the membrane. TiO_2(−) and Au(−) showed greater adsorption potential than Ag(−), which was not removed by adsorption even at the highest membrane areas. Even though all three of these NPs had the same carboxyl-group functionality, the core NP material was still important for the NP-membrane interactions.

Both of the positively charged NPs [TiO_2(+) and Au(+)] were readily removed by even the smallest membrane areas in adsorption experiments. Adsorption on the glass vials and/or caps was also apparent for TiO_2(+), as the NP concentration in the control

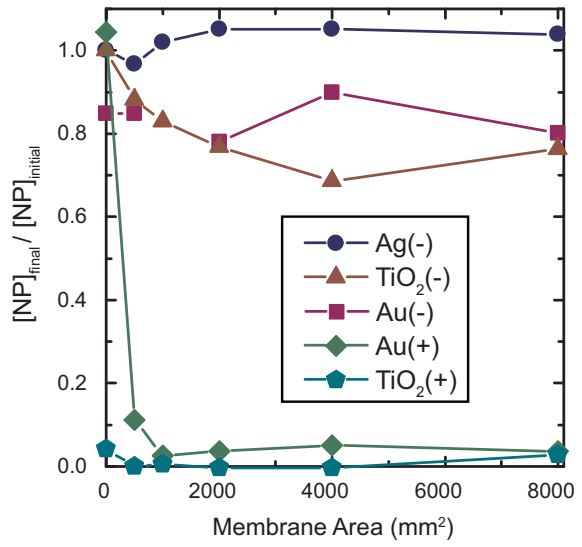

Fig. 2. Concentration remaining after 24 h of exposure of NP solutions to 0.1 μm PVDF membranes in adsorption experiments. Measured initial concentrations (as metal) were 0.32, 0.28, 0.41, 0.16, and 0.08 ppm for Ag(−), TiO_2(−), Au(−), Au(+), and TiO_2(+), respectively.

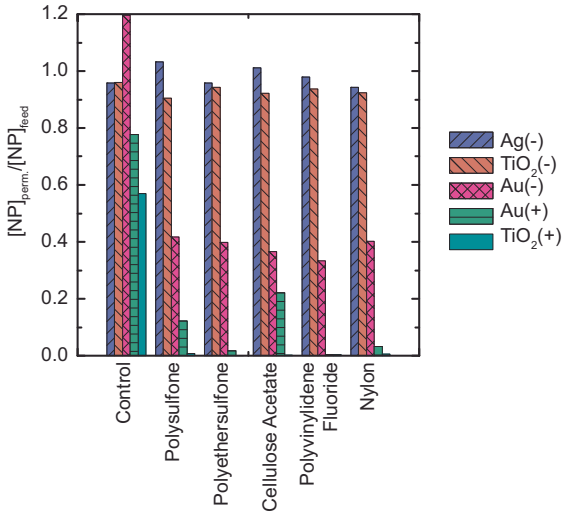

Fig. 3. Normalized permeate concentrations of NPs passed ten times through syringe filters (0.22-μm pore size) made of five different polymeric materials. Control samples were passed through the filtration device with no membrane present.

sample (zero membrane area) was significantly lowered compared to the feed solution. These experiments clearly indicate that positively charged NPs readily sorb to negatively charged membranes and other surfaces.

3.3. Syringe filtration

The dead-end filtration tests described above were carried out with 0.1-μm membranes. For studying interactions between NPs and larger pore-size (0.22-μm) membranes, syringe filtration was used. Fig. 3 shows the syringe filtration results, reported as $[NP]_{permeate}/[NP]_{feed}$. The control sample included the syringes (2), tubing, and filter holder without a membrane. Controls indicated that some removal of NPs (especially positively charged NPs) was due to adsorption on the apparatus even though NPs were pre-adsorbed as described in Section 2. The elevated control concentration for Au(+) could be due to resuspension of NPs deposited during that pre-adsorption step.

Ag(−) and TiO_2(−) behaved similarly in syringe filtration experiments; both had 0–10% removal (i.e., $[NP]_{permeate}/[NP]_{feed}$ ratios of 0.9–1.0). Approximately 60% of the Au(−) was removed for all membrane types. Positively charged NPs had greater removals (i.e., lower $[NP]_{permeate}/[NP]_{feed}$ ratios); TiO_2(+) was removed almost completely whereas Au(+) showed between 78 and 100% removal.

Overall, differences in the rejection of NPs by the five different 0.22-μm membrane materials were minimal. Even though the membrane surface zeta potentials were somewhat variable (Table 2), there was no correlation between rejection and membrane charge; retention was dominated by NP rather than membrane properties. The potential implication for water treatment or other applications is that most polymeric membranes may behave similarly. Further understanding the NP properties will be critical to predict retention performance.

3.4. Centrifugal filtration

With 0.1-μm and higher pore size membranes, passage by negatively charged NPs clearly occurred. Therefore, the use of tighter UF membranes, with MWCOs from 3 to 100 kDa, was investigated. For all five UF membranes, rejection of all NPs was between 90 and 100%, with the notable exception of Ag(−) (Fig. 4a). Ag(−) rejection averaged 90% for 3-, 10-, and 30-kDa membranes but was

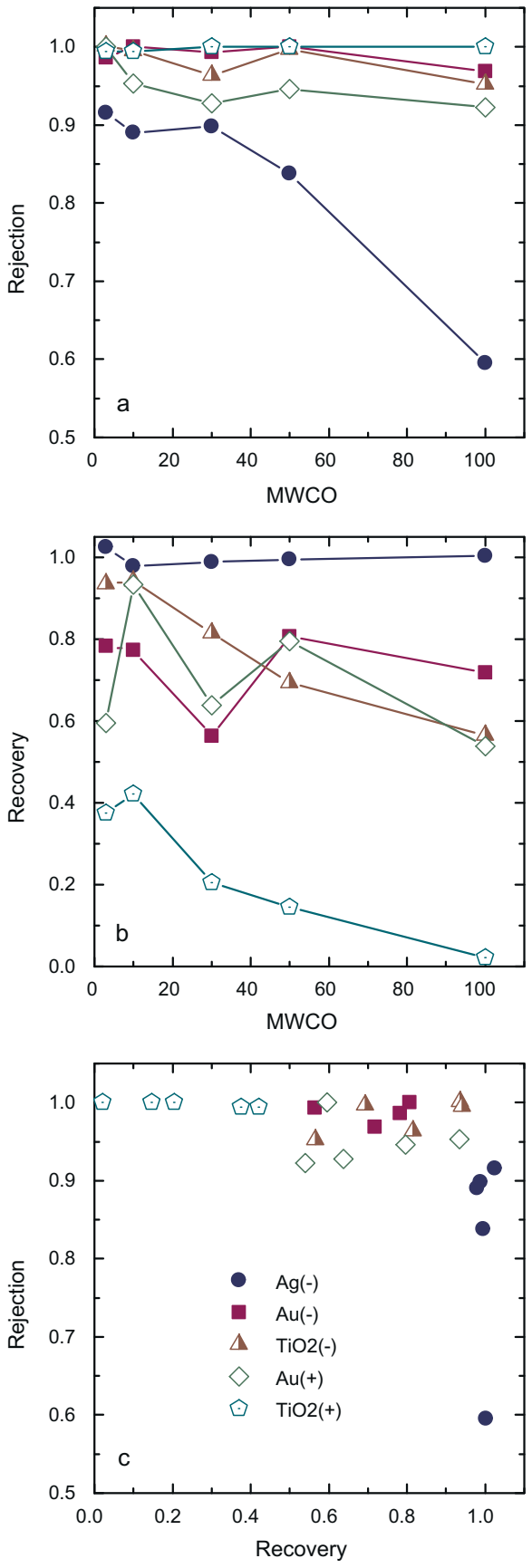

Fig. 4. (a) Rejection vs. MWCO, (b) recovery vs. MWCO and (c) rejection vs. recovery for centrifugal filtration experiments. Measured feed concentrations (as metal) were 0.36, 0.32, 0.27, 0.086 and 0.17 ppm for Ag(−), TiO_2(−), Au(−), Au(+), and TiO_2(+), respectively.

only 84% for the 50-kDa case and 60% for the 100-kDa case. As noted previously, the ion-selective electrode measurements indicated the presence of 14% dissolved Ag that would be expected to pass through the 3-, 10-, and 30-kDa membranes; thus, these membranes rejected Ag(−) NPs completely. For the 50- and 100-kDa membranes, however, Ag(−) NPs were able to permeate.

For the other NPs, trends in rejection among UF membranes were not as apparent. Au(−), TiO_2(−), and TiO_2(+) rejection was greater than 90% in all cases. TiO_2(+) was rejected to the greatest degree, near 100% in all cases.

Recovery was evaluated to understand if NPs were rejected on the basis of size exclusion alone or if they were sorbed onto the membrane or trapped in the membrane pores. As described in Section 2, high recovery (close to 1) would be expected when NPs had weak adsorptive interaction potential or were not easily entrapped in the membrane pores. Low recovery is expected for particles that adsorb strongly to the membrane or are trapped in the pores. These trends are evident in the recovery data (Fig. 4b). Ag(−) recovery was near 100% in all cases, which is consistent with it having the lowest adsorption affinity. Approximately 93% of the TiO_2(−) was recovered with 3- and 10-kDa membranes, but only 82%, 70%, and 58% with the looser 30-, 50-, and 100-kDa membranes, respectively. This suggests that TiO_2(−) could not enter the pores of the tighter membranes but was able to penetrate and become internally attached to the looser UF membranes. The Au(−) and Au(+) data contain more scatter, and trends are not readily observed.

The NP that consistently was shown to have the greatest adsorption affinity and was the easiest to reject, TiO_2(+), also had the lowest recovery. The trend of lower recovery at larger pore size was again evident with this NP, suggesting that entrapment within the larger pores likely occurred.

Plotting rejection vs. recovery (Fig. 4c) reveals an interesting way to observe differences among NP types. The Ag(−) data points form a vertical elongated cluster on the lower right of the plot, and the TiO_2(+) points form a horizontal elongated cluster on the upper left. The other NPs are also grouped, and these groups overlap near the upper right. Such a plot reveals that rejection and recovery are inherently connected; NPs with higher rejection tended to have lower recovery. It also demonstrates visually that Ag(−) and TiO_2(+) NPs were the most different, so their plotted groups did not overlap, whereas the other NPs were more similar to one another. This is interesting given that the UF membranes were of varying pore size; were a single membrane to be used, the distinction among NP types would be clearer. The rejection vs. recovery analysis seems to be a promising method for characterizing NPs. As work progresses toward determining the physicochemical properties of NPs and understanding how those properties change when released to the environment [39] or used in applications, the rejection vs. recovery analysis could be one tool to connect those properties with transport behavior.

3.5. Overall NP behavior

The discussion above was divided into sections for each filtration type. It is also useful to discuss the results in terms of NP type. Ag(−) NPs were the least prone to adsorption, so they were the least retained, even passing to a large extent through the 50- and 100-kDa membranes. The actual pore size of those membranes is difficult to quantify, and in reality there exists a distribution of sizes necessitating knowledge of not only the average, but also the standard deviation [40]; this is the reason that manufacturers typically report the more operationally suitable MWCO values. But on the basis of work by others, the pore sizes for the 50 and 100-kDa membranes can be estimated as 7 and 9 nm, respectively [40] (where the geometric standard deviation of the pore sizes (σ) is assumed to be 1.4). Thus the Ag(−) NPs, which have a median particle size between about 6 and 7 nm, exhibited some passage through membranes that had roughly the same pore size (7 and 9 nm).

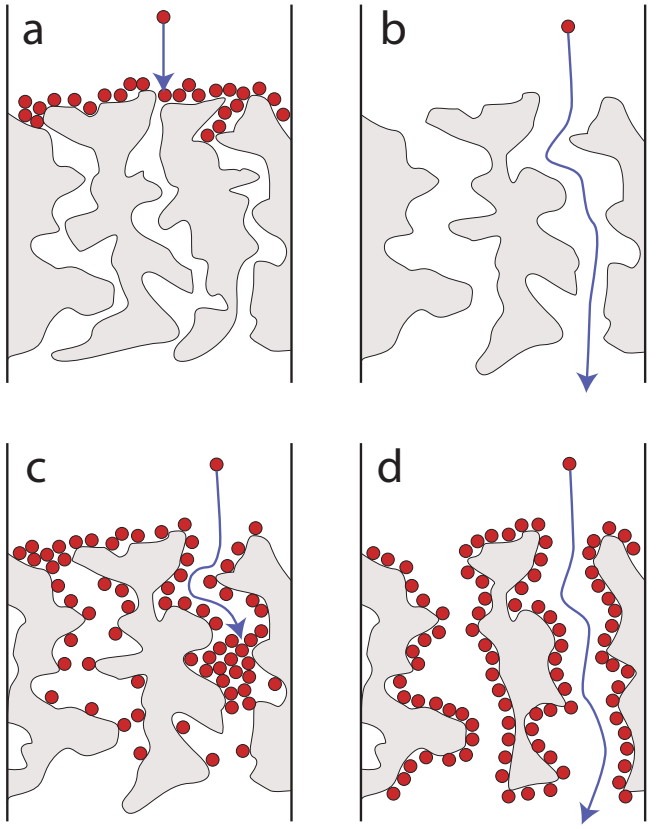

Fig. 5. Idealized categories of nanoparticle interactions with porous membranes. (a) NPs are larger than pores, resulting in size exclusion, (b) NPs are smaller than pores, resulting in NP passage, (c) NPs are smaller than pores, but adsorptive interactions cause pore blockage and (d) NPs are smaller than pores, and the pores are large enough that even when adsorption causes initial NP rejection, breakthrough eventually occurs.

TiO_2(−) and Au(−) were similar to one another in terms of NP-membrane adsorption affinity (Fig. 2), which was verified by their similar behavior in recovery measurements from centrifugal filters (Fig. 4b). It is interesting, then, that Au(−) was retained to a much greater extent than TiO_2(−) in both dead-end and syringe filtration experiments (Figs. 1 and 3, respectively). One possible explanation is that Au(−) had greater NP–NP self-adsorption affinity than TiO_2(−). Thus, in rejection experiments with pores larger than the NPs, initial Au(−) NP deposition (even if low) led to attachment of more NPs that adsorbed to the already-deposited materials. The difference between Au(−) and TiO_2(−) could also be explained by aggregation occurring with Au(−), but not with TiO_2(−), which would depend again on Au(−) having a higher NP–NP self-adsorption affinity.

For positively charged NPs the strong NP-membrane adsorption affinity meant that adsorption was the dominant mechanism and the NPs were well rejected in all cases. However, breakthrough at the end of the filter run (as discussed in Section 3.6) indicates that NP–NP self-adsorption affinity was not strong enough to keep the NPs retained.

3.6. Interaction mechanisms

We propose that the interaction mechanisms between NPs and porous membranes can be classified into four categories. In the first category, membrane pores are smaller than the NPs, and size

exclusion results (Fig. 5a). This occurred for all of the NPs with the smallest-pore-size UF membranes (3- and 10-kDa).

In the second category, the membrane pores are larger than the NPs and little or no adsorption affinity exists so that complete NP passage occurs (Fig. 5b). This was the predominant situation for Ag(−) NPs with 0.1- and 0.22-μm membranes. TiO_2(−) behaved similarly with the MF membranes, although it displayed some adsorption affinity.

The third category occurs when the membrane pores are larger than the NPs, but adsorptive interactions cause pore constriction, blockage or decreased passage (Fig. 5c). This was the dominant situation in the data presented here, such as for Au(−), Au(+), and TiO_2(+) on 0.1- and 0.22-μm membranes and 30-kDa and larger UF membranes. TiO_2(−) also appeared to be rejected because of adsorptive pore blocking on the larger-pore-size UF membranes (50 and 100 kDa). Adsorptive pore blocking is most apparent for pores that are close to the NP size.

The final category of interaction mechanisms occurs when adsorptive interactions cause NP retention, but the membrane pores are significantly larger than the NPs. The pores are not completely blocked, and breakthrough subsequently occurs. This mechanism was less obvious than the others but was most apparent in the Au(−) filtrations on 0.1-μm membranes (Fig. 1), which demonstrated an increase in passage toward the end of the experiment. Similar increases in NP concentration over filtration time were observed in other experiments shown in the supplementary data (Fig. S6).

The four categories of interaction mechanisms are idealized and not mutually exclusive. For example, even though Ag(−) NPs did not show a measurable adsorption affinity and were significantly smaller than the 0.1-μm pore size membranes, some removal occurred at the beginning of the 0.1 μm filtration. The pores are not homogeneous or round, so entrapment of some material and blockage of smaller pores and crevices could occur at the beginning; once they are filled, complete NP passage begins. The phenomenon can then be thought of as fitting Fig. 5d, even though entrapment occurs instead of true adsorption. TiO_2(−) exhibited a similar entrapment effect on 0.1-μm membranes, but adsorption was also likely. The other NPs should have been entrapped as well, but adsorption was stronger and thus more important.

An analogy can be drawn here between NP-membrane interactions and the behavior of other compounds with membranes. Studies of pharmaceutical rejection by nanofiltration (NF) membranes point to three important mechanisms: steric (size) exclusion, electrostatic repulsion, and adsorption [41]. These mechanisms are expected for NP rejection by MF and UF membranes but may lead to different effects. Electrostatic repulsion increases small-molecule rejection in NF membranes but may decrease NP rejection in MF/UF membranes (when the particles are smaller than the pores) because the NPs will flow through the pores rather than attach to the walls. Adsorption of small-molecule organics in NF membranes results in enhanced rejection at the beginning of the filtration cycle, but then rejection is diminished over time as the membrane becomes saturated and breakthrough occurs [42]. A similar situation may occur with NPs and MF/UF membranes when the pores are large enough, but adsorption may increase rejection of NPs in MF and UF membranes with smaller pores because the adsorbed particles can cause pore constriction and blockage.

While the focus of this work is on understanding NP rejection, these experiments also give insight into membrane fouling. An often-cited way of describing fouling phenomena is that of Hermia [43] who delineated four mechanisms: cake filtration, intermediate blocking, standard blocking, and complete blocking. Our first NP interaction category (Fig. 5a) is analogous to Hermia's cake filtration mechanism, where particles accumulate on top of the membrane. Our second interaction category (Fig. 5b) is a non-fouling case, since particles pass through without accumulating on the membrane. Our third category (Fig. 5c) is analogous to Hermia's "intermediate blocking" mechanism, where flux decline occurs due to both pore constriction and pore blocking, depending on the size of the pores and the particles. Our fourth category is analogous to Hermia's "standard blocking" mechanism where fouling is due to pore constriction.

While the four interaction categories described here are consistent with the data collected, it should be noted that there are limitations to this categorization. One limitation is that the difference between adsorption and entrapment could not be teased out of these data for all membrane pore sizes. Entrapment in UF centrifugal filtration could be observed by comparing recoveries for different pore sizes, but since recovery could not be measured so easily for larger pore-size membranes, there is no way to distinguish adsorption from entrapment. Another limitation is that we do not know if NPs are truly embedded in the membrane pores or if they remain attached to the membrane surface. We attempted to determine this via recovery measurements, but advanced transmission electron microscopy or other characterization tools would be needed to be certain about where the NPs actually collect. A final limitation in this study lies in the inability to collect adequate flux data using these experimental techniques. Flux information would be useful for further elucidating the interaction mechanisms, and for analyzing fouling mechanisms by Hermia's theory. Flux was recorded for the 1-L dead-end filtration experiments, but the data (Fig. S7) were inadequate to draw conclusions and adsorption to the filtration apparatus by positively charged NPs (as mentioned previously) may have skewed the results. When the volume was reduced to 60 ml for better control and quantification of rejection, there was no observable flux decline. For centrifugal and syringe filtrations, flux could not be measured due to the nature of those setups. Future experiments designed to collect flux information would be valuable.

4. Conclusions

From these experiments, five main conclusions can be drawn about the interactions of this class of functionalized NPs with polymeric MF and UF membranes.

(1) All of the functionalized NPs were well rejected by membranes with pores smaller than the NP size, but some were well removed by membranes with larger pores. This occurred when NP-membrane adsorption affinity was high, as in the case of positively charged NPs being electrostatically attracted to the negatively charged membranes.
(2) Even though NP-membrane adsorption affinity was similar for two NPs [TiO_2(−) and Au(−)] their rejection behavior with MF membranes was quite different. This could be due to differences in the NP–NP self-adsorption affinity, or aggregation potential. Au(−) appeared to have a higher NP–NP self-adsorption affinity, resulting in capture of incoming NPs by already deposited NPs and thus increasing the overall removal.
(3) Five different polymeric membranes (polysulfone, polyethersulfone, cellulose acetate, polyvinylidenefluoride, and nylon) behaved very similarly in terms of rejection. The NP properties appeared to be more important for determining transport behavior than the membrane properties.
(4) Centrifugal filtration apparatuses facilitate measurement of both NP rejection and recovery where recovery is defined as the fraction of NPs collected on the membrane that can be easily rinsed away from the surface. Plotting rejection vs. recovery could be a useful tool to characterize NP behavior and distinguish NP types one from another.

(5) The behavior of these functionalized NPs can be described by four categories or scenarios displayed graphically in Fig. 5. These categories are (a) membrane pores smaller than the membrane leading to complete NP retention, (b) pores larger than the NPs and NPs with low adsorption affinity leading to NP passage, (c) pores similar in size to the NPs and adsorption leading to pore blockage and NP retention, and (d) pores being large enough that even when adsorption occurs the pores remain open and NPs eventually break through. The four categories of interactions are not mutually exclusive.

Acknowledgements

This work was supported by the NIH Grand Opportunities (RC2) program through NIEHS grant DE-FG02-08ER64613. Assistance from an undergraduate researcher (Amanda Hernandez) and technician (Marisa Masles) are greatly appreciated. Characterization of nanoparticles was conducted within the LeRoyEyring Center for Solid State Science.

Appendix A. Supplementary data

Supplementary data associated with this article can be found, in the online version, at doi:10.1016/j.jhazmat.2011.11.051.

References

[1] T. Benn, B. Cavanagh, K. Hristovski, J.D. Posner, P. Westerhoff, The release of nanosilver from consumer products used in the home, J. Environ. Qual. 39 (2010) 1875–1882.
[2] T.M. Benn, P. Westerhoff, Nanoparticle silver released into water from commercially available sock fabrics, Environ. Sci. Technol. 42 (2008) 4133–4139.
[3] S. Chae, E.M. Hotze, Y. Xiao, J. Rose, M.R. Wiesner, Comparison of methods for fullerene detection and measurements of reactive oxygen production in cosmetic products, Environ. Eng. Sci. 27 (2010) 797–804.
[4] L. Geranio, M. Heuberger, B. Nowack, The behavior of silver nanotextiles during washing, Environ. Sci. Technol. 43 (2009) 8113–8118.
[5] S.F. Hansen, E.S. Michelson, A. Kamper, P. Borling, F. Stuer-Lauridsen, A. Baun, Categorization framework to aid exposure assessment of nanomaterials in consumer products, Ecotoxicology 17 (2008) 438–447.
[6] N.C. Mueller, B. Nowack, Exposure modeling of engineered nanoparticles in the environment, Environ. Sci. Technol. 42 (2008) 4447–4453.
[7] F. Gottschalk, T. Sonderer, R.W. Scholz, B. Nowack, Modeled Environmental concentrations of engineered nanomaterials (TiO_2, ZnO, Ag, CNT, Fullerenes) for different regions, Environ. Sci. Technol. 43 (2009) 9216–9222.
[8] F. Gottschalk, R.W. Scholz, B. Nowack, Probabilistic material flow modeling for assessing the environmental exposure to compounds: methodology and an application to engineered nano-TiO_2 particles, Environ. Model. Softw. 25 (2010) 320–332.
[9] M.A. Kiser, P. Westerhoff, T. Benn, Y. Wang, J. Perez-Rivera, K. Hristovski, Titanium nanomaterial removal and release from wastewater treatment plants, Environ. Sci. Technol. 43 (2009) 6757–6763.
[10] N. O'Brien, E. Cummins, Nano-scale pollutants fate in irish surface and drinking water regulatory systems, Hum. Ecol. Risk Assess. 16 (2010) 847–872.
[11] T.M. Scown, R. van Aerle, C.R. Tyler, Review do engineered nanoparticles pose a significant threat to the aquatic environment? Crit. Rev. Toxicol. 40 (2010) 653–670.
[12] X. Li, D.W. Elliott, W. Zhang, Zero-valent iron nanoparticles for abatement of environmental pollutants: materials and engineering aspects, Crit. Rev. Solid State Mater. Sci. 31 (2006) 111–122.
[13] A. Zhang, M. Zhou, L. Han, Q. Zhou, The combination of rotating disk photocatalytic reactor and TiO_2 nanotube arrays for environmental pollutants removal, J. Hazard. Mater. 186 (2011) 1374–1383.
[14] T.H. Bae, T.M. Tak, Effect of TiO_2 nanoparticles on fouling mitigation of ultrafiltration membranes for activated sludge filtration, J. Membr. Sci. 249 (2005) 1–8.
[15] J.D. Fowlkes, M.J. Doktycz, P.D. Rack, An optimized nanoparticle separator enabled by electron beam induced deposition, Nanotechnology 21 (2010) 165303.
[16] D. Jassby, S. Chae, Z. Hendren, M. Wiesner, Membrane filtration of fullerene nanoparticle suspensions: effects of derivatization, pressure, electrolyte species and concentration, J. Colloid Interface Sci. 346 (2010) 296–302.
[17] A. Jawor, E.M.V. Hoek, Removing Cadmium ions from water via nanoparticle-enhanced ultrafiltration, Environ. Sci. Technol. 44 (2010) 2570–2576.
[18] M.M. Zhang, L.F. Song, Mechanisms parameters affecting flux decline in cross-flow microfiltration and ultrafiltration of colloids, Environ. Sci. Technol. 34 (2000) 3767–3773.
[19] E.M.V. Hoek, A.S. Kim, M. Elimelech, Influence of cross flow membrane filter geometry and shear rate on colloidal fouling in reverse osmosis and nanofiltration separations, Environ. Eng. Sci. 19 (2002) 357–372.
[20] E.M.V. Hoek, S. Bhattacharjee, M. Elimelech, Effect of membrane surface roughness on colloid–membrane DLVO interactions, Langmuir 19 (2003) 4836–4847.
[21] J. Brant, A. Childress, Membrane–colloid interactions: comparison of extended DLVO predictions with AFM force measurements, Environ. Eng. Sci. 19 (2002) 413–427.
[22] J.A. Brant, A.E. Childress, Colloidal adhesion to hydrophilic membrane surfaces, J. Membr. Sci. 241 (2004) 235–248.
[23] K.J. Kim, V. Chen, A.G. Fane, Ultrafiltration of colloidal silver particles - flux, rejection, and fouling, J. Colloid Interface Sci. 155 (1993) 347–359.
[24] K.J. Kim, V. Chen, A.G. Fane, Characterization of clean and fouled membranes using metal colloids, J. Membr. Sci. 88 (1994) 93–101.
[25] A.I. Schafer, U. Schwicker, M.M. Fischer, A.G. Fane, T.D. Waite, Microfiltration of colloids and natural organic matter, J. Membr. Sci. 171 (2000) 151–172.
[26] T.D. Waite, A.I. Schafer, A.G. Fane, A. Heuer, Colloidal fouling of ultrafiltration membranes: impact of aggregate structure and size, J. Colloid Interface Sci. 212 (1999) 264–274.
[27] J.R. Stephens, J.S. Beveridge, A.H. Latham, M.E. Williams, Diffusive flux and magnetic manipulation of nanoparticles through porous membranes, Anal. Chem. 82 (2010) 3155–3160.
[28] H.C. Poynton, J.M. Lazorchak, C.A. Impellitteri, M.E. Smith, K. Rogers, M. Patra, K.A. Hammer, H.J. Allen, C.D. Vulpe, Differential gene expression in daphnia magna suggests distinct modes of action and bioavailability for ZnO nanoparticles and Zn ions, Environ. Sci. Technol. 45 (2011) 762–768.
[29] E. Navarro, F. Piccapietra, B. Wagner, F. Marconi, R. Kaegi, N. Odzak, L. Sigg, R. Behra, Toxicity of silver nanoparticles to Chlamydomonas reinhardtii, Environ. Sci. Technol. 42 (2008) 8959–8964.
[30] N. Nishida, S. Ichikawa, N. Toshima, Simple and environmentally compatible one-pot synthesis of Au nanoparticles from bulk: separation of Au, Ag, and Cu in water, Chem. Lett. 38 (2009) 1082–1083.
[31] S. Liu, X. Wei, M. Chu, J. Peng, Y. Xu, Synthesis and characterization of iron oxide/polymer composite nanoparticles with pendent functional groups, Colloids Surf. B: Biointerfaces 51 (2006) 101–106.
[32] S. Laurent, D. Forge, M. Port, A. Roch, C. Robic, L.V. Elst, R.N. Muller, Magnetic iron oxide nanoparticles: Synthesis, stabilization, vectorization, physicochemical characterizations, and biological applications, Chem. Rev. 108 (2008) 2064–2110.
[33] N.S. Wigginton, K.L. Haus, M.F. Hochella Jr., Aquatic environmental nanoparticles, J. Environ. Monit. 9 (2007) 1306–1316.
[34] T.M. Tsao, M.K. Wang, P.M. Huang, Automated ultrafiltration device for efficient collection of environmental nanoparticles from aqueous suspensions, Soil Sci. Soc. Am. J. 73 (2009) 1808–1816.
[35] D.L. Grzenia, J.O. Carlson, S.R. Wickramasinghe, Tangential flow filtration for virus purification, J. Membr. Sci. 321 (2008) 373–380.
[36] M.J. Steuck, Porous membrane having hydrophilic surface and process. 06/676,681 (1984).
[37] M. Momtaz, J.L. Dewez, J. Marchand-Brynaert, Chemical reactivity assay and surface characterization of a poly(vinylidene fluoride) microfiltration membrane (Durapore DVPP), J. Membr. Sci. 250 (2005) 29–37.
[38] D.B. Mosqueda-Jimenez, R.M. Narbaitz, T. Matsuura, Membrane fouling test: apparatus evaluation, J. Environ. Eng. -Asce. 130 (2004) 90–99.
[39] K.L. Chen, B.A. Smith, W.P. Ball, D.H. Fairbrother, Assessing the colloidal properties of engineered nanoparticles in water: case studies from fullerene C-60 nanoparticles and carbon nanotubes, Environ. Chem. 7 (2009) 10–27.
[40] J. Ren, Z. Li, F. Wong, A new method for the prediction of pore size distribution and MWCO of ultrafiltration membranes, J. Membr. Sci. 279 (2006) 558–569.
[41] L.D. Nghiem, A.I. Schafer, M. Elimelech, Pharmaceutical retention mechanisms by nanofiltration membranes, Environ. Sci. Technol. 39 (2005) 7698–7705.
[42] K. Kimura, G. Amy, J.E. Drewes, T. Heberer, T.U. Kim, Y. Watanabe, Rejection of organic micropollutants (disinfection by-products, endocrine disrupting compounds, and pharmaceutically active compounds) by NF/RO membranes, J. Membr. Sci. 227 (2003) 113–121.
[43] J. Hermia, Constant pressure blocking filtration laws - application to power-law non-Newtonian fluids, Trans. Inst. Chem. Eng. 60 (1982) 183–187.